Article

Functionalizing Diatomite-Based Micro-Arc Coatings for Orthopedic Implants: Influence of TiO_2 Addition

Alexander D. Kashin[1], Mariya B. Sedelnikova[1,*], Pavel V. Uvarkin[1], Anna V. Ugodchikova[1,3], Nikita A. Luginin[1], Yurii P. Sharkeev[1,2], Margarita A. Khimich[4], Olga V. Bakina[4]

[1] Laboratory of Physics of Nanostructured Biocomposites, Institute of Strength Physics and Materials Science of SB RAS, Tomsk, 634055, Russia; smasha5@yandex.ru (M.B.S.), kash@ispms.ru (A.D.K.), uvarkin@ispms.tsc.ru (P.V.U.), sharkeev@ispms.ru (Y.P.S.), nikishek90@gmail.com (N.A.L.), ugodch99@gmail.com (A.V.U.)

[2] Research School of High-Energy Physics, National Research Tomsk Polytechnic University, Tomsk, 634050, Russia; sharkeev@ispms.ru (Y.P.S.)

[3] Laboratory of plasma synthesis of materials, Troitsk Institute for Innovation & Fusion Research, Moscow Region, Troitsk, 108840, Russia; ugodch99@gmail.com (A.V.U.)

[4] Laboratory of nanobioengineering, Institute of Strength Physics and Materials Science of SB RAS, Tomsk, 634055, Russia; ovbakina@ispms.tsc.ru (O.V.B.), khimich@ispms.tsc.ru (M.A.K.)

* Correspondence: smasha5@yandex.ru

Abstract: The method of micro-arc oxidation has been utilized to synthesize a protective biocompatible coating for a bioresorbable orthopedic Mg implant. This paper presents the results of a comprehensive research of micro-arc coatings based on diatomite – a biogenic material consisting of shells of diatom microalgae. The main focus of this study was the functionalization of diatomite-based micro-arc coatings by incorporating the particles of titania (TiO_2) into them. Various properties of the resulting coatings were examined and evaluated. The XRD analysis has revealed the formation of a new magnesium orthosilicate phase – forsterite (Mg_2SiO_4). It has been established that the corrosion current density of the coatings has decreased by 2-4 orders of magnitude after the inclusion of TiO_2 particles, depending on the coating process voltage. The adhesion strength of the coatings has increased following the particle incorporation. The processes of dissolution of both coated and uncoated samples in a sodium chloride solution were studied. The *in vitro* cell viability was assessed, which showed that the coatings significantly reduce the cytotoxicity of Mg samples.

Keywords: Orthopedic implants, magnesium alloy, micro-arc coating, diatomite, TiO_2, *in vitro* biocompatibility, corrosion resistance

1. Introduction

In recent years, magnesium and its alloys have become increasingly popular in the field of medical materials science. In particular, magnesium can be used as a material for the fabrication of bioresorbable orthopedic implants. This is feasible due to its low specific gravity (≈1.74 g/cm3), high biocompatibility, and elastic modulus close to that of human cortical bone (≈40–45 GPa) [1–6]. Such a modulus of elasticity virtually eliminates the risk of the stress shielding effect that can lead to undesirable consequences in the form of the onset of osteopenia at the implant site [7–9]. According to Wolff's law, the bone in a healthy human or animal adapts to the stresses to which they are subjected [10]. If the load on the bone decreases, the bone becomes less dense and weaker due to the lack of incentive needed to continue remodeling. Therefore, magnesium is a very promising material in this respect.

However, magnesium also has certain disadvantages associated with its excessive susceptibility to corrosive media, as well as the active release of hydrogen at the site of contact between the implant and the surrounding tissues [11–14]. To address these challenges, this paper proposes modifying the implant surface with a protective, biologically active coating based on natural diatomite functionalized with titanium dioxide particles.

 doi:10.20944/preprints202306.0150.v1

To synthesize the coatings, the micro-arc oxidation (MAO, also known as plasma electrolytic oxidation – PEO) method was implemented. This method is characterized by coating a valve metal substrate submerged in a bath of electrolyte. Under the influence of a strong electric field, numerous plasma micro-arc discharges are formed on the surface of the substrate, contributing to intensive electrochemical interaction of the electrolyte components with the substrate material and, consequently, the formation of a protective oxide coating [15,16]. This coating acts as a two-way solution. On the one hand, it protects the magnesium implant from being dissolved too quickly by creating a barrier between it and the aggressive environment [17–20]. On the other hand, it enables and facilitates the osseointegration process between the implant and the bone tissue [21–25].

The most widely used coatings in the field of micro-arc coating research are the ones synthesized in electrolytes based on phosphates, silicates, and, a little less common, aluminates [26–33]. Aluminate-based electrolytes are typically used to produce wear resistant MAO coatings due to the dominant formation of $MgAl_2O_4$ as a very solid phase. Phosphate- and silicate-based electrolytes are commonly used to synthesize coatings with improved corrosion resistance, which is due to the high corrosion resistance of Mg_2SiO_4 and $Mg_3(PO_4)_2$, respectively. [34]. Such coatings can be further functionalized by the addition of insoluble particles to the composition of an electrolyte. These can include various pharmaceutical products, carbides, nitrides, oxides, etc. [35–43]. Altering the concentration and/or proportions of these particles makes it possible to control and tailor the structure and various properties of the resulting coatings.

In this work, an electrolyte based on biogenic diatomite, which had already been used in our earlier studies [44], was used as the base electrolyte. The distinction of this work is the modification of a diatomite-based coating with titanium oxide particles added to the base electrolyte in the form of a dispersed phase. Analysis of the scientific literature on this topic shows that the addition of titanium dioxide particles changes the structure and properties of micro-arc coatings, increasing their corrosion resistance, wear resistance and antibacterial properties [45–50]. Ergo, the addition of TiO_2 particles is a promising direction in the field of functionalization of micro-arc coatings.

The main objective of this study is to investigate the effect of adding refractory titanium oxide particles on the structure and various properties of protective, biologically active micro-arc coatings for bioresorbable orthopedic Mg implants.

2. Materials and Methods

As a substrate material, high-purity magnesium alloy MA2-1hp (AZ31 alloy equivalent) (VILS, Moscow, Russia) was chosen. Its chemical composition is as follows (wt. %):

- 94.12 Mg;
- 4.05 Al;
- 1.1 Zn;
- 0.6 Mn
- >0.1 other elements combined.

The alloy has a Young's modulus of 42 GPa and a density of 1.790 kg/m^3, based on the manufacturer's tests. Model samples for the coating deposition were cut from a solid piece of magnesium alloy by the method of electric discharge machining. After that, the samples were ground with a 600-grit abrasive sandpaper (Hermes Schleifmittel GmbH, Germany) to achieve the surface roughness Ra of 0.5-0.6 μm. Following this, the samples were deep-cleaned using an ultrasonic cleaner (Elmasonic S, Elma, Germany) filled with distilled water and ethanol sequentially for 30 minutes each.

The electrolyte for the coating deposition included NaOH, Na_2SiO_3, NaF dissolved in distilled water and dispersed phases of diatomite ($SiO_2 \cdot nH_2O$) and titania (TiO_2). The diffractogram of TiO_2 powder is shown in Figure 1. The diffractogram of diatomite powder has been provided previously in [44].

Preprints (www.preprints.org) | NOT PEER-REVIEWED | Posted: 2 June 2023 doi:10.20944/preprints202306.0150.v1

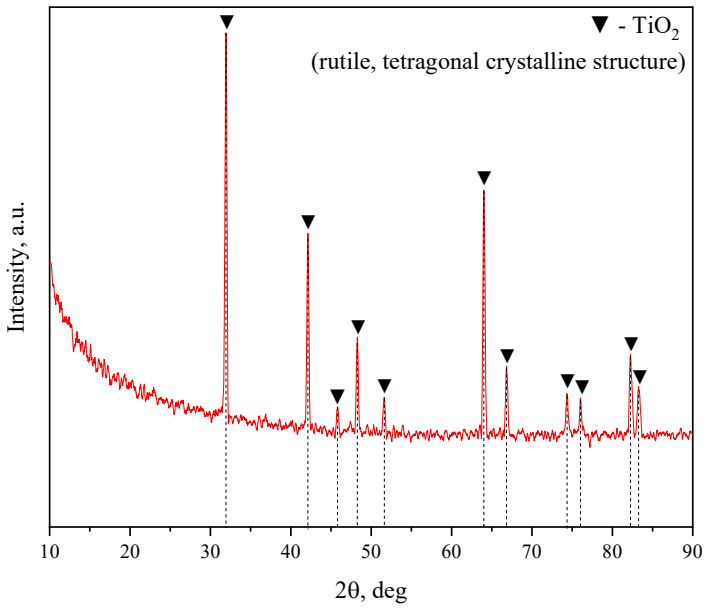

Figure 1. X-ray diffraction pattern of the initial TiO_2 powder.

The coatings were synthesized via the method of micro-arc oxidation. For the coating deposition process, the anodic potentiostatic mode was implemented with a pulse frequency and duration of 50 Hz and 100 μs, respectively. The coatings were deposited for 5 minutes at four different pulsed voltages: 350, 400, 450, and 500 V. To carry out the experiment, a "Micro-Arc 3.0" equipment was used, which consisted of a direct current (DC) power supply, a water-cooled electrolyte bath, and counter-electrodes. The monitoring of the parameters during the MAO process was carried out with the help of the equipment's built-in software. A magnetic mixer stirred the electrolyte continuously during the process to agitate the solution and prevent the particle aggregation.

The surface morphology and the elemental composition of the resulting coatings were studied using a LEO EVO 50 scanning electron microscope (Zeiss, Germany), equipped with an INCA x-act EDX spectrometer (Oxford Instruments, UK).

Changes in the phase composition of the coatings depending on the deposition voltage were investigated via an X-ray diffractometer (DRON–7, Burevestnik, Russia) with the following parameters: CoK_α radiation, 35 kV voltage, 22 mA tube current, and 2θ angle range of 10° to 90° with 0.02° scanning step.

The adhesion strength of the coatings was assessed using a Revetest RST scratch tester (CSM Instruments, USA) equipped with a diamond indenter 200 μm in radius. The indenter scratched the surface of the sample, moving at a speed of 1 mm/min, while the load was increasing linearly. The length of the scratch was 5 mm. The peak indentation force was 40 N and the loading rate was 3.9 N/min.

Corrosion resistance of the coatings in comparison with uncoated Mg alloy was determined using the "P-40X" electrochemical workstation (Electrochemical Instruments, Russia). A 0.9% NaCl solution was used as the electrolyte in a three-electrode cell, where a graphite rod served as a counter electrode and an Ag/AgCl electrode was used as a reference electrode. The exposed sample surface area equaled to 1 cm^2. The scan rate at which the potentiodynamic polarization curves were obtained equaled to 2 mV/s. The electrode potential ranged from –1.9V to +1.9V. The temperature of the electrolyte was maintained at 37 °C to simulate the conditions under which a coated implant would function in a human body.

The method of immersion was used to determine the biodegradation rate of both the coated and uncoated Mg specimens. The samples were immersed in a 0.9% NaCl physiological saline solution in compliance with ISO 10993-5. The experiment was conducted over the course of 14 days.

The following formula (1) has been used to calculate the mass loss of the specimens:

Preprints (www.preprints.org) | NOT PEER-REVIEWED | Posted: 2 June 2023 doi:10.20944/preprints202306.0150.v1

$$\Delta m = \frac{m_0 - m_i}{m_0} \cdot 100\%, \quad (1)$$

where m_0 is the sample mass before dissolution, mg, m_i – after dissolution, mg.

The condition of the coatings at certain stages of the experiment was visually assessed via MET 1MT optical microscope (Altami, Russia).

The biocompatibility of samples was examined *in vitro* using MTT assay after direct contact of the cells with the testing material. The NIH/3T3 cell line was purchased from the State Research Center of Virology and Biotechnology "VECTOR" (Novosibirsk, Russia). The cells were seeded in a flask with DMEM (Lonza, Switzerland) with 10% fetal bovine serum (HyClone, USA) and 5% penicillin/streptomycin-glutamine (HyClone, USA) and incubated at 37 °C in a 5% CO_2. After 24 h incubation period the attached cells were trypsinizated for 3–5 min and centrifuged at 1400 rpm for 5 min. The cell culture was seeded into 24-well culture plates (total volume of 2 ml) at 70000 cells per well. Test samples were placed in each well. Cells were incubated for 24 hours at 37 °C in a 5% CO_2. Cells that were incubated in the medium without the sample present were used as a control.

The viability of the cells after exposure was analyzed using MTT assay [44]. In typical procedure, 200 µl of MTT [3-(4, 5-dimetheylthiazol-2)-2, 5 diphenyl tetrazolium bromide] solution was added to each well. The plates were incubated for 4 h at 37 °C in a 5% CO_2. Then the MTT-containing medium was removed and the cells were treated by adding 100 µL DMSO (HyClone, USA) to dissolve the formazan crystal. In the final step, the optical density (OD) of solution was recorded at 570 nm wavelength using a microplate reader Thermo Scientific Multiskan FC (Thermo Fisher Scientific, USA). The measured OD value was used to calculate the relative cell viability (%) according to eq. (1) :

$$\text{Cell viability (\%)} = \text{OD (test sample)}/\text{ OD (control)} \times 100 \quad (2)$$

Each experiment was done in duplicate. All statistical analyses were performed using the statistical software package STATISTICA 10.0. The normal distribution of the results was checked by the Kolmogorov-Smirnov test. The significance of differences in mean values between groups was analyzed using the Mann-Whitney test. Differences were considered significant at $p < 0.05$.

3. Results and discussion

3.1. Coating thickness and roughness

Figure 2 displays the thickness and roughness of the coatings in relation to MAO process voltage. The thickness of deposited coatings increases exponentially, which correlates well with our previous studies related to diatomite-based coatings [44,51]. The surface roughness ranges from 2.5 to 5 µm, with a sharp increase at 450 V. This is due to the more intense course of the micro-arc oxidation process at higher voltages, which leads to a greater number of micro-arc plasma discharges on the substrate surface. This, in turn, leads to the merging of many small microdischarges into one large electric arc, leading to a more active intumescence of the surface, and, accordingly, to the formation of a rougher topography.

Preprints (www.preprints.org) | NOT PEER-REVIEWED | Posted: 2 June 2023 doi:10.20944/preprints202306.0150.v1

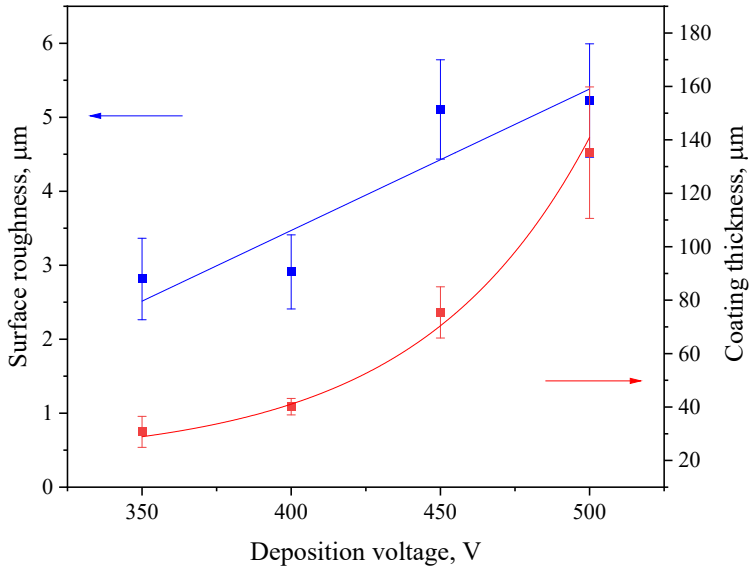

Figure 2. Roughness (red line) and thickness (blue line) of coatings deposited at four different MAO process voltages

3.2. Morphology and pore structure

The visual analysis of the SEM micrographs of the coatings obtained at different process voltages has been carried out (Fig. 3 a-d). It was revealed that the coatings have a large number of variously shaped pores, ranging in size from 100 nm to 12 μm. We can observe the fragments of lithified diatomeae shells both on the surface and within the bigger pores. Some of the fragments were partially melted into the matrix of the coating, thus giving it an ordered reticulated pore structure. Unmelted particles of both diatomite and titania are also present in substantial amounts on the surface of the coating. It is worth noting, however, that the number of unmelted particles decreases with the increase in deposition process voltage. This can be explained by a larger quantity of more powerful micro-arc discharges being generated during the MAO process at higher voltages, which leads to a more active disintegration and fusion of the oxide particles into the coating matrix.

In addition, Figure 3 (c, d, g, h) presents the micrographs of cross-sections of the coatings. The analysis of the microphotographs leads to the conclusion that the coatings have an internal porous structure, including pores of different types and sizes. The coatings deposited at MAO voltages of 350 and 400 V contain large pores, up to 5 μm in diameter, indicating single high-intensity micro-arc discharges (Figure 3 c,d). Groups of small pores less than 1 μm in size are scattered around them, resulting from cascades of micro-arc discharges. As the voltage of the MAO process increases to 450-500 V, the thickness of the coatings increases significantly, but the nature of the internal pore structure does not change; both large and small pores, evenly distributed throughout the coating thickness, are present in the coatings (Figure 3 g,h). The pores are mostly enclosed, but in some cases channeled pores resulting from a powerful breakdown of the coating are observed (Figure 3 g). In addition, the presence of TiO_2 particles can be observed in the cross sections of the coatings.

Preprints (www.preprints.org) | NOT PEER-REVIEWED | Posted: 2 June 2023 doi:10.20944/preprints202306.0150.v1

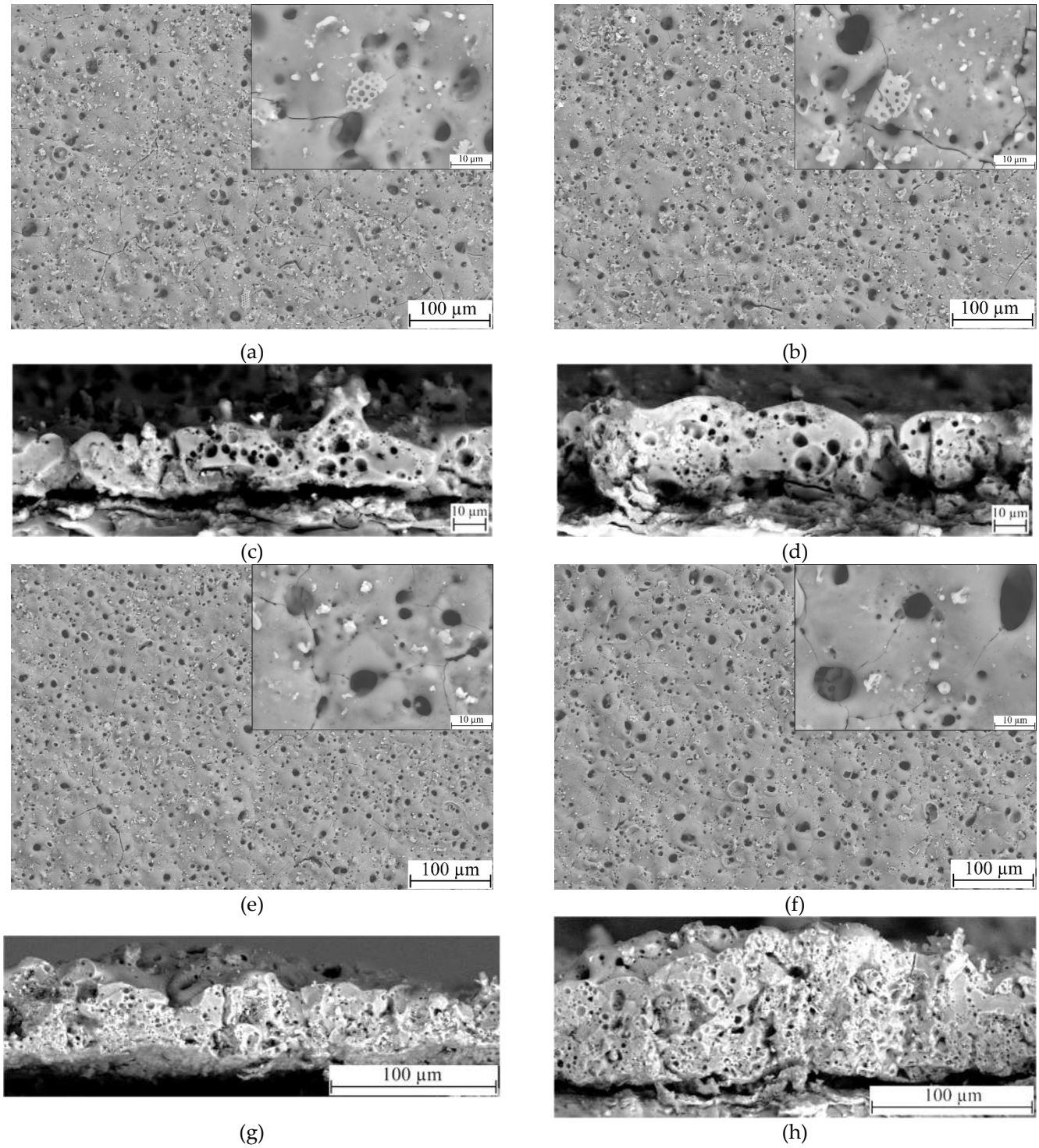

Figure 3. SEM micrographs of the surfaces and cross-sections of TiO_2-doped diatomite coatings synthesized at different process voltages: (a,c) – 350 V, (b,d) – 400 V, (e,g) – 450 V, (f,h) – 500 V. Mag.: 500x, 5000x for a, b, e, f; 2000x for c, d; 1000x for g, h.

3.3. Elemental composition

To characterize the chemical composition of the synthesized coatings, the method of energy dispersive X-ray microanalysis has been used. Figure 4 shows the maps of element distribution as well as the sum spectrum of the elements present in the coating. High localized concentrations of Ti and Si were detected via element mapping, correlating to titania and diatomite particles, respectively. Table 1 displays the amount of each element (in at. %) in relation to the coating deposition voltage. It can be concluded that the amount of most elements remains approximately the same regardless of the process voltage. The exceptions are silicon and titanium, the amount of which decreases as the

Preprints (www.preprints.org) | NOT PEER-REVIEWED | Posted: 2 June 2023 doi:10.20944/preprints202306.0150.v1

MAO voltage increases. This can be partially attributed to fewer particles of both diatomite and titania remaining unmelted on the coatings surface at higher MAO voltages, as can be seen in Fig. 3.

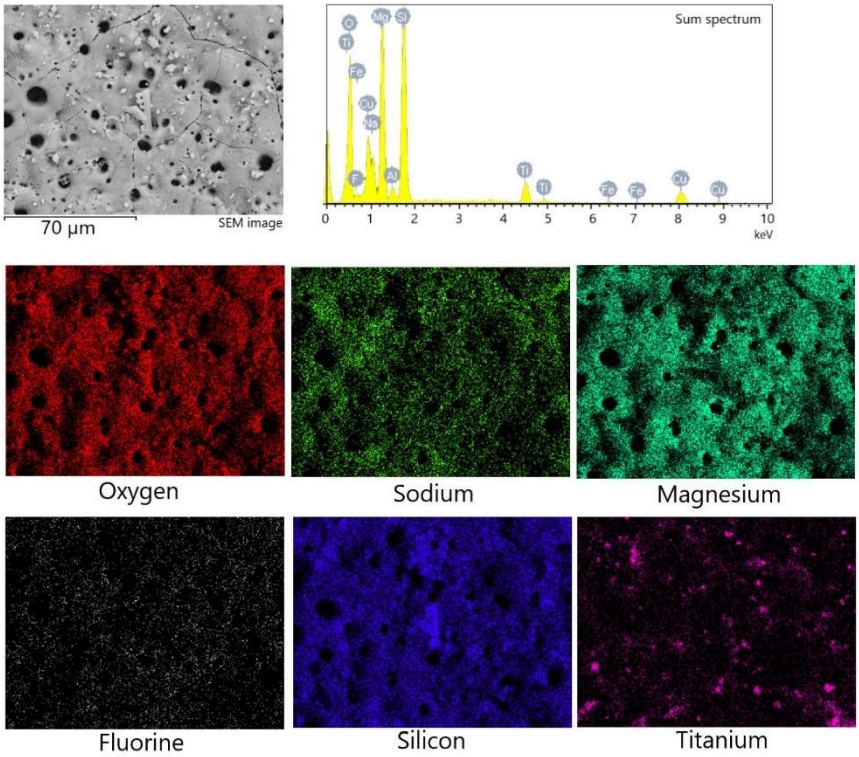

Figure 4. Energy dispersive X-ray analysis of the TiO_2-incorporated diatomite coating formed at 500 V: SEM image, sum spectrum, and element mapping

Table 1. Chemical composition of the coatings, at. %

Element	350 V	400 V	450 V	500 V
O Kα	58.7±2.5	62.2+1.7	60.7±1.7	61.3±0.6
F Kα	4.1±0.9	3.9±1.3	5.2±0.8	4.72±0.5
Na Kα	1.4±0.4	1.8±0.2	2.1±0.6	2.1±0.3
Mg Kα	14.8±1.8	12.9±1.3	14.3±2.6	14.49±0.6
Al Kα	0.9±0.1	0.8±0.0	0.8±0.1	0.84±0.0
Si Kα	17.2±1.2	15.6±0.4	14.7±0.6	14.8±0.2
Ti Kα	2.9±0.2	2.6±0.7	2.2±0.6	1.82±0.2

The EDX analysis of the element distribution in the cross section of the coating (Figure 5) showed that the elements O and Si are evenly distributed throughout the coating thickness, while Mg and F are mainly concentrated closer to the substrate in the transition layer, and the Na concentration, on the contrary, is higher in the surface layer. In addition, isolated local Ti accumulations are observed, confirming the presence of TiO_2 particles in the coating volume.

Preprints (www.preprints.org) | NOT PEER-REVIEWED | Posted: 2 June 2023 doi:10.20944/preprints202306.0150.v1

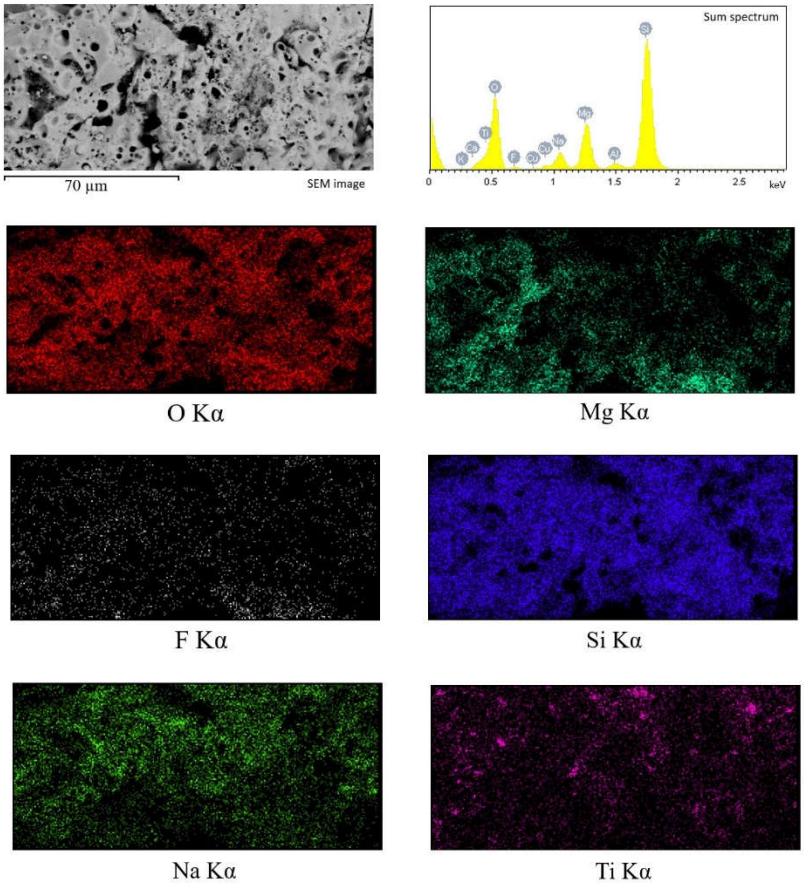

Figure 5. Energy dispersive X-ray analysis of the cross-sections of TiO_2-incorporated diatomite coating formed at 450 V: SEM image, sum spectrum, and element mapping

The chemical composition of the cross sections of the coatings formed at different voltages of the MAO process (Table 2) is almost identical to the composition of the surface of these coatings presented in Table 1. In the cross-sections of the coatings applied at voltages of 350-400 V, a higher content of F is noted, but with an increase in voltage, its amount decreases. There is also a decrease in Mg concentration when the process voltage is increased to 450-500 V.

Table 2. Chemical composition of the coatings (cross-section), at. %

Element	350 V	400 V	450 V	500 V
O Kα	57.2±1.5	59.8±0.4	62.4±1.3	61.6±2.5
F Kα	8.0±0.8	5.6±1.0	4.1±0.9	3.8±0.7
Na Kα	0.5±0.08	1.0±0.1	2.9±0.8	3.0±0.7
Mg Kα	14.5±1.6	14.6±1.0	9.7±0.8	11.0±3.6
Al Kα	0.4±0.2	0.7±0.1	0.6±0.1	0.6±0.0
Si Kα	17.5±0.1	16.7±0.5	18.5±1.2	17.8±2.1
Ti Kα	1.7±0.3	1.4±0.6	1.5±0.3	2.0±1.0

3.3.1. X-ray diffraction analysis

Figure 6 showcases the X-ray diffraction patterns for the TiO_2-augmented diatomite coatings formed at four different process voltages. The formation of a new predominant phase has been detected in all four coatings – forsterite (Mg_2SiO_4) (ICDD #34-0189), which is a magnesium

Preprints (www.preprints.org) | NOT PEER-REVIEWED | Posted: 2 June 2023 doi:10.20944/preprints202306.0150.v1

orthosilicate from the olivine group of minerals. We can also see the reflexes correlating to both magnesium (ICDD #35-0821) and its oxide – periclase (ICDD #45-0946). The incorporation of TiO_2 particles into the coating has resulted in a few peaks corresponding to rutile (ICDD #21-1276), which is the most common natural form of titanium dioxide.

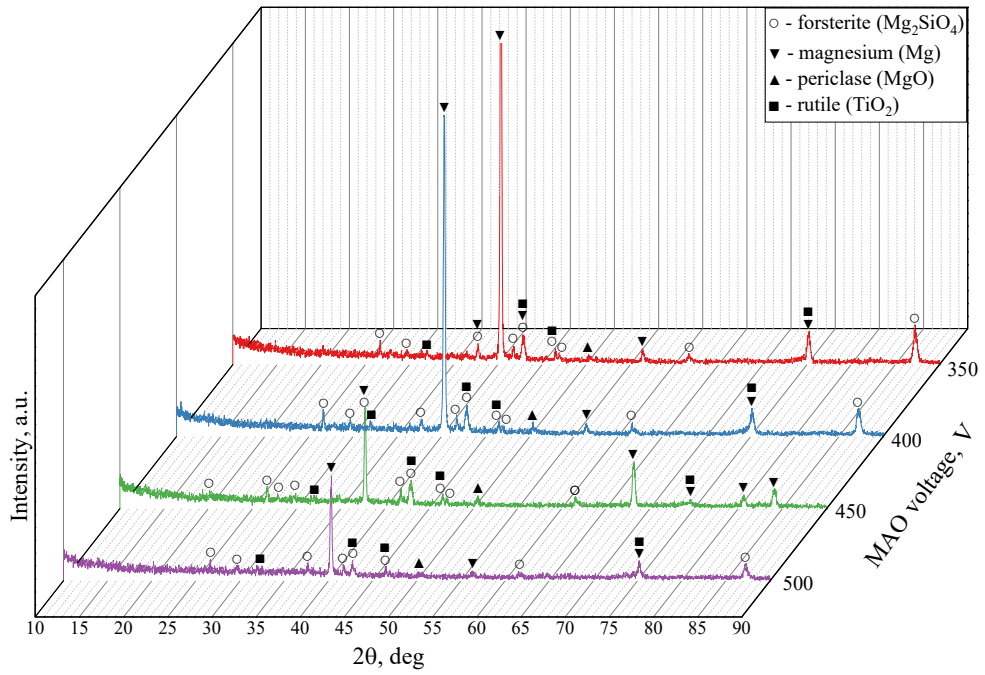

Figure 6. X-ray diffraction patterns of the coatings formed at 350, 400, 450, 500 V.

3.4. Mechanical properties

3.4.1. Scratch testing

The results of the study of the mechanical properties of TiO_2-augmented diatomite coatings, performed by scratch testing, showed that they have a very high adhesion strength. Figure 7 shows the optical images of the coatings, applied at different voltages of the MAO process, after scratch testing. On scratches, it is possible to distinguish the zone of destruction of the coating at the moment of penetration of the indenter to the substrate – this is a solid light zone at the end of the scratch. But for the coatings applied at 500 V this zone is practically absent, which indicates the highest adhesion strength of these coatings.

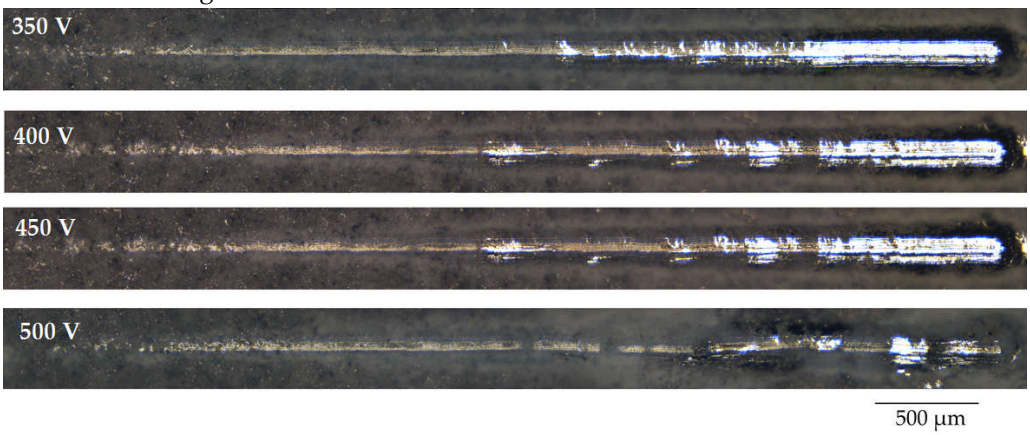

Figure 7. Optical images of the scratches obtained as a result of testing the coatings deposited at different MAO voltages.

Preprints (www.preprints.org) | NOT PEER-REVIEWED | Posted: 2 June 2023 doi:10.20944/preprints202306.0150.v1

The determination of the critical load at failure confirmed these results. A diagram of the critical load versus voltage at which the coating was formed is shown in Figure 8a. The figure shows that the critical load values for coatings applied at 350-450 V are approximately the same, ranging from 24.0-25.4 N. However, the coating applied at 500V is characterized by the highest critical load value of 35.2 N. The results obtained in previous studies show that diatomite-based coatings without TiO_2 particles have much lower adhesion strength. The maximum critical load did not exceed 10 N [44].

Since the thickness of the coatings increases exponentially with an increase in the stress of the MAO process, we assume that the adhesive strength of the coatings depends on their thickness.

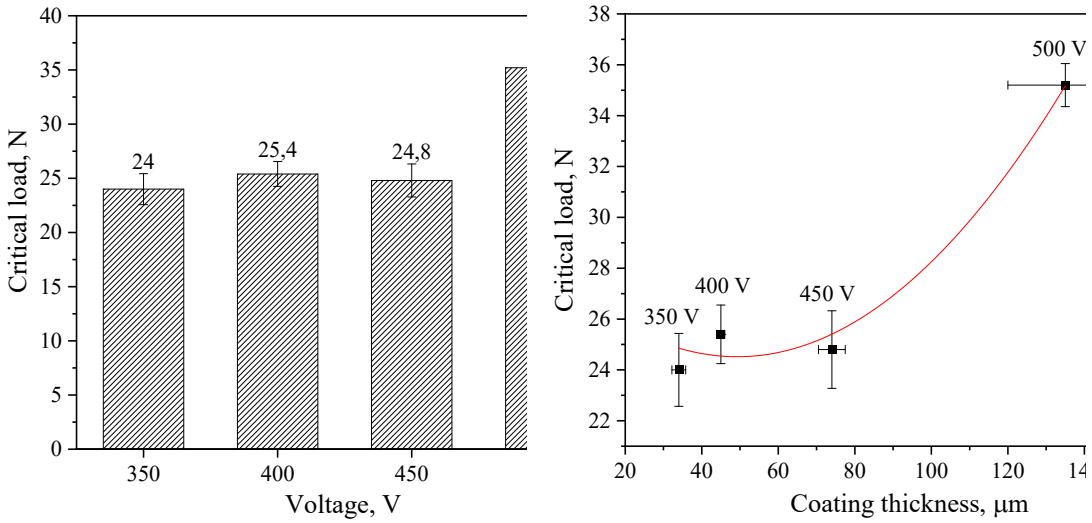

(a) (b)

Figure 8. Diagram of correlation between the critical load and the MAO voltage (a); graph of the correlation dependence of the critical load on the thickness of coatings formed at different voltages (b)

Figure 8b shows a correlation graph of the dependence of the critical load on the thickness of the coatings, indicating that this dependence has an exponential character, which confirms our assumption.

3.5. Electrochemical properties

One of the main objectives of this study was to improve the corrosion properties of diatomite-based coatings by incorporating titanium oxide particles into them. This is especially relevant for aggressive media, in particular, the liquid component of the physiological medium of the human body. Figure 9 shows the potentiodynamic polarization curves for both pure magnesium samples and samples with coatings applied at different voltages. It can be seen that the coatings deposited at 350 and 450 V are the most resistant to corrosion. The values of polarization resistance R_P for these samples amounted to 1.22×10^8 A·cm^{-2} and 1.41×10^8 A·cm^{-2}, respectively.

Preprints (www.preprints.org) | NOT PEER-REVIEWED | Posted: 2 June 2023 doi:10.20944/preprints202306.0150.v1

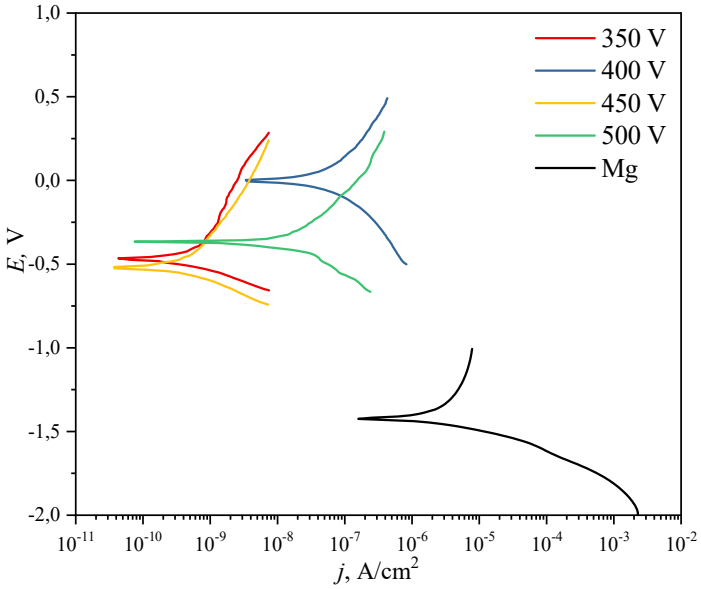

Figure 9. Potentiodynamic polarization (PDP) curves of the studied samples.

A comparative analysis of the corrosion resistance of diatomite coatings before [44] and after the addition of titanium dioxide particles showed that the addition of particles increases the polarization resistance of coatings by 1-4 orders of magnitude, depending on the coating deposition voltage. The corrosion current density in this case decreases by 1 to 3 orders of magnitude. Overall, the corrosion current density of TiO_2-doped samples decreased by 2-4 orders of magnitude compared to uncoated Mg samples, and the polarization resistance, respectively, increased by 2-4 orders of magnitude. The experimental data are given in Table 2.

Table 3. Comparative table of electrochemical parameters of the samples before [44] and after the addition of TiO_2 particles

Sample	Diatomite			Diatomite + TiO_2		
	E_c, V	J_c, A cm^{-2}	R_p, Ω cm^2	E_c, V	J_c, A cm^{-2}	R_p, Ω cm^2
Mg	–	–	–	-1.43	2.25×10^{-6}	1.61×10^{4}
350V	–0.13	3.08×10^{-7}	6.69×10^{4}	-0.46	3.30×10^{-10}	1.22×10^{8}
400V	–0.98	1.78×10^{-7}	8.83×10^{4}	-0.02	4.01×10^{-8}	1.65×10^{6}
450V	–1.55	8.70×10^{-7}	2.1×10^{4}	-0.52	4.01×10^{-10}	1.41×10^{8}
500V	–1.58	7.62×10^{-8}	6.83×10^{5}	-0.36	1.32×10^{-8}	4.21×10^{6}

3.6. Bioresorption study

The processes of dissolution of both coated and uncoated alloy samples were studied for 11 days while kept in 0.9% NaCl solution (Figure 10). Studies have shown that when a magnesium alloy is dissolved, three periods can be distinguished. The first period – during the first 4 days, the dissolution rate of the alloy is lower than the dissolution rate of samples with coatings. After 4 days, the dissolution rate increases sharply and exceeds the dissolution rate of the coated samples. After 8 days, the dissolution rate slightly decreases again. As described in previous studies, the dissolution rate of magnesium alloy directly depends on two processes: the first is the dissolution of alloy components, the second is the process of reverse precipitation of dissolution products (magnesium hydroxide $Mg(OH)_2$) on the alloy surface. If the first process prevails - the dissolution rate increases, if the second process prevails - the alloy dissolves more slowly.

Preprints (www.preprints.org) | NOT PEER-REVIEWED | Posted: 2 June 2023 doi:10.20944/preprints202306.0150.v1

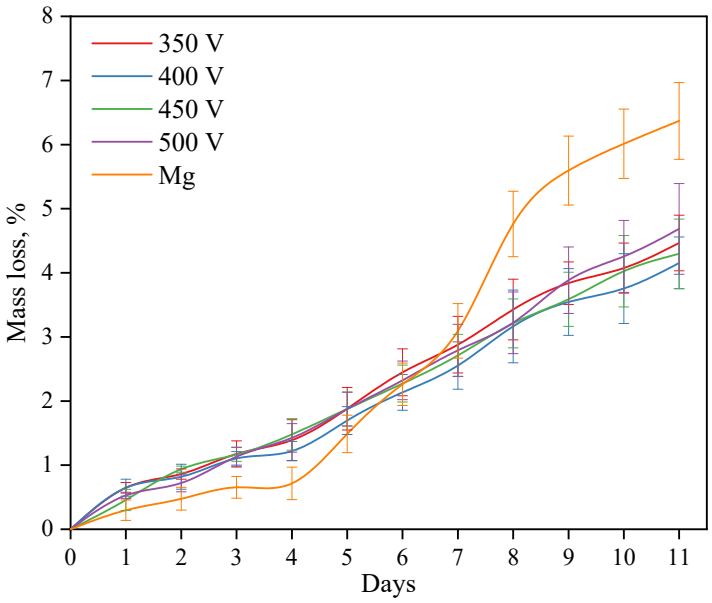

Figure 10. Graph of the samples mass loss depending on the time of immersion in the 0.9% NaCl solution.

The rate of dissolution of coatings of all types is constant and linear. After 6 days of dissolution, the mass loss of the coated samples becomes less than that of magnesium alloy. The intensity of the dissolution of the coating does not depend on the voltage of the MAO process at which the coating was applied.

The optical images of the samples before dissolution and after 4, 8, and 11 days of dissolution were also analyzed (Figure 11). On the surface of the pure magnesium alloy, the precipitation of dissolution products is observed after 4 days of incubation in 0.9% NaCl solution. The amount of dissolution products on the surface of the alloy increases with an increase in the duration of incubation. Similar patterns were observed and described in previous studies [44, 51].

As the optical images show, the dissolution of the coatings occurs in the area of surface structure defects (pores, cracks). An increase in the diameter and depth of the pores can be noted. But the morphology of the coatings surface does not change significantly, which indicates the resistance of this type of coatings to dissolution in the biological environment. This phenomenon is explained by the presence of insoluble compounds such as magnesium silicate (forsterite) and oxides of magnesium and titanium in the coatings.

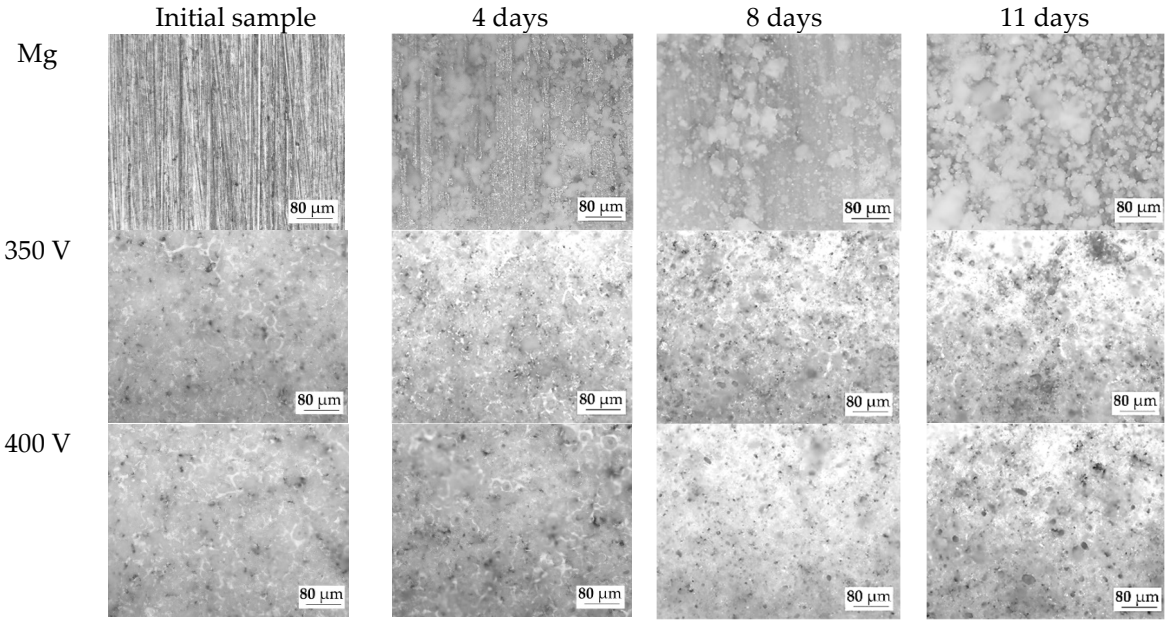

Preprints (www.preprints.org) | NOT PEER-REVIEWED | Posted: 2 June 2023 doi:10.20944/preprints202306.0150.v1

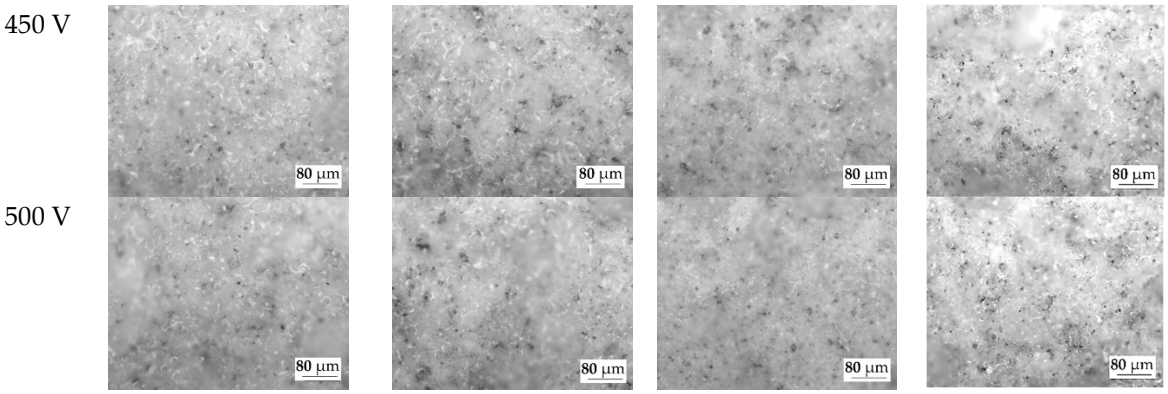

Figure 11. Optical microscopic images of the samples at different stages of the bioresorption process.

3.7. In vitro cytotoxicity

The cell viability was assessed using the MTT assay and quantified according to eq. 2. Compared to the control, Coating 400 V and Coating 500 V treated cells showed no statistically significant decrease in viability, cell viabilities were about 94% and 98% of the control, respectively (Figure 12). At the same time, the Mg alloy treated 3T3 cells showed decreased viability and the cell viability was about 43% (high toxicity). Based on these results, it is safe to say that the coatings significantly reduce the toxicity of the samples.

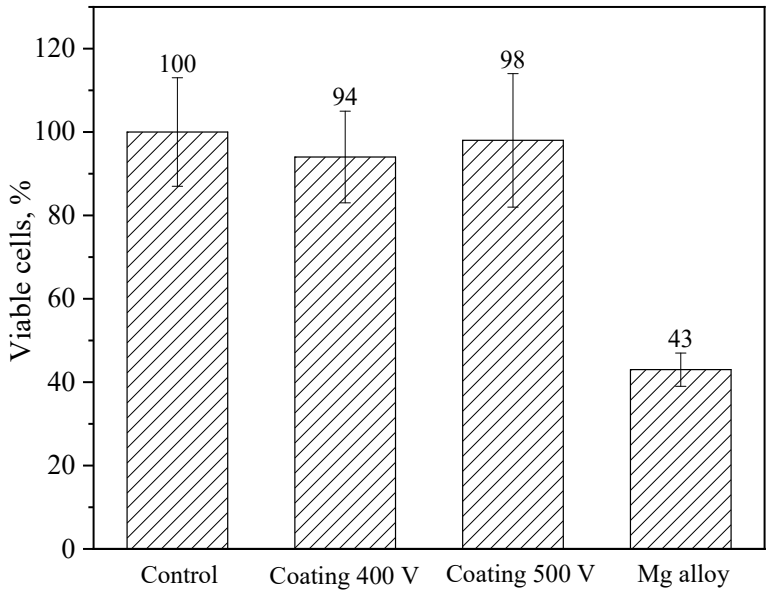

Figure 12. Results of *in vitro* NIH/3T3 cell viability measured by an MTT assay after 24-h culturing with negative control (DMEM), as well as with Mg alloy (positive toxic control) or samples coated at 400 V and 500 V.

4. Conclusions

The coatings considered in this article are suitable for use as a biocompatible and bioactive protectant for magnesium-based bioresorbable orthopedic implants. The micro-arc oxidation method was used to synthesize coatings based on diatomite with the addition of titanium dioxide particles. A range of 350 to 500 V was chosen as the optimal voltage range of the MAO process. Depending on the MAO voltage, the thickness of the coating varied from approximately 30 to 140 µm, and the roughness values lay within 2.5 – 5 µm range.

The resulting coatings were studied using a number of research methods, including scanning electron microscopy (SEM), energy-dispersive X-ray microanalysis (EDX), X-ray diffraction analysis

 doi:10.20944/preprints202306.0150.v1

(XRD), scratch testing, potentiodynamic polarization testing, *in vitro* immersion method, *in vitro* MTT assay.

It has been found that the morphology of the coatings is comprised of a large number of pores of various shapes and sizes, fragments of lithified diatomeae shells, and unmelted particles of both diatomite and TiO_2. Some diatom algae fragments were partially fused into the coating matrix, giving it a reticulated pore structure. The X-ray diffraction analysis has revealed the formation of a new prevalent phase – forsterite (Mg_2SiO_4). Peaks corresponding to magnesium and periclase (MgO), as well as rutile (TiO_2), were also observed in the diffraction patterns of the resulting coatings. The coatings have demonstrated a very high adhesion strength (critical load equaled to 24 – 35 N) as compared to diatomite-based coatings without the addition of TiO_2 particles (critical load <10 N). The corrosion resistance of the coatings has been assessed, which revealed that the coatings synthesized at 350 and 450 V had the highest values of polarization resistance at 1.22×10^8 $A\cdot cm^{-2}$ and 1.41×10^8 $A\cdot cm^{-2}$, respectively. Diatomite-based coatings, the composition of which included TiO_2 particles, had 1-4 orders of magnitude greater polarization resistance than coatings without the addition of titanium dioxide particles. The *in vitro* immersion method was implemented to study the dissolution rate of both the coated and uncoated samples, which has shown that the dissolution rate of all coated samples regardless of the deposition voltage has a linear character. The mass loss rate of uncoated Mg samples exceeds that of the coated samples after 4 days of immersion and amounts to more than 6% at the end of the experiment. 3T3 mouse fibroblasts were used to assess the *in vitro* cytotoxicity of the coatings, i.e. cell viability during the contact with the coating. The coatings synthesized at 400 and 500 V have exhibited no statistically significant decrease in viability of the cells, amounting to 94% and 98% cell survival rate, which indicates high biocompatibility of diatomite-based TiO_2-augmented coatings.

Author Contributions: Conceptualization, M.B.S. and A.D.K.; investigation, A.D.K., P.V.U., N.A.L., A.V.U., M.A.K. and O.V.B.; validation, M.B.S., A.D.K. and O.V.B.; formal analysis, A.D.K., A.V.U., M.A.K. and P.V.U.; resources, Y.P.S.; data curation, P.V.U.; writing—original draft preparation, A.D.K.; writing—review and editing, M.B.S. and A.D.K.; visualization, A.D.K.; supervision, M.B.S. and Y.P.S.; project administration, M.B.S.; funding acquisition, M.B.S. All authors have read and agreed to the published version of the manuscript.

Funding: The research was funded by the Russian Science Foundation, grant No. 23-29-00141, https://rscf.ru/en/project/23-29-00141/.

Data Availability Statement: Not applicable.

Acknowledgments: The authors are grateful to A.I. Tolmachev from the Institute of Strength Physics and Materials Science SB RAS (Tomsk, Russia) for his assistance in the preparation of experimental materials.

Conflicts of Interest: The authors declare no conflict of interest.

References

1. Chakraborty Banerjee, P.; Al-Saadi, S.; Choudhary, L.; Harandi, S.E.; Singh, R. Magnesium Implants: Prospects and Challenges. *Materials* **2019**, *12*, 136. doi.org/10.3390/ma12010136
2. Jhamb, S.; Matai, J.; Marwaha, J.; Goyal, A.; Pandey, A. A comprehensive analysis on magnesium-based alloys and metal matrix composites for their in-vitro biocompatibility. *Advances in Materials and Processing Technologies* **2022**, 1-34. doi.org/10.1080/2374068X.2022.2113521
3. Uppal, G.; Thakur, A.; Chauhan, A.; Bala, S. Magnesium based implants for functional bone tissue regeneration – A review. *Journal of Magnesium and Alloys* **2022**, *10*, 356-386. doi.org/10.1016/j.jma.2021.08.017
4. Song, J.; She, J.; Chen, D.; Pan, F. Latest research advances on magnesium and magnesium alloys worldwide. *Journal of Magnesium and Alloys* **2020**, *8*, 1-41. doi.org/10.1016/j.jma.2020.02.003
5. Shahin, M.; Munir, K.; Wen, C.; Li, Y. Magnesium matrix nanocomposites for orthopedic applications: A review from mechanical, corrosion, and biological perspectives. *Acta Biomaterialia* **2019**, *96*, 1-19. doi.org/10.1016/j.actbio.2019.06.007
6. Hassan, S.F.; Islam, M.T.; Saheb, N.; Baig, M.M.A. Magnesium for Implants: A Review on the Effect of Alloying Elements on Biocompatibility and Properties. *Materials* **2022**, *15*, 5669. doi.org/10.3390/ma15165669
7. Baskerville, S.J.J. Effects of orthopedic implant and host bone properties on stress-shielding induced osteopenia. Doctoral dissertation, Florida Institute of Technology, Melbourne, FL, May 2022.

8. Schwartz, C. How to reduce osteopenia in total knee arthroplasty?. *Eur J Orthop Surg Traumatol* **2019**, *29*, 139–145. doi.org/10.1007/s00590-018-2290-z
9. Savio, D.; Bagno, A. When the Total Hip Replacement Fails: A Review on the Stress-Shielding Effect. *Processes* **2022**, *10*, 612. doi.org/10.3390/pr10030612
10. Wolff, J. The classic: on the inner architecture of bones and its importance for bone growth. 1870. *Clin Orthop Relat Res* **2010**, 468, 1056-65. doi.org/10.1007/s11999-010-1239-2
11. Wang, J.; Dou, J.; Wang, Z.; Hu, C.; Yu, H.; Chen, C. Research progress of biodegradable magnesium-based biomedical materials: A review. *Journal of Alloys and Compounds* **2022**, *923*, 166377. doi.org/10.1016/j.jallcom.2022.166377
12. Atrens, A.; Shi, Z.; Mehreen, S.U.; Johnston, S.; Song, G.-L.; Chen, X.; Pan, F. Review of Mg alloy corrosion rates. *Journal of Magnesium and Alloys* **2020**, *8*, 989-998. doi.org/10.1016/j.jma.2020.08.002
13. Feliu, S., Jr. Electrochemical Impedance Spectroscopy for the Measurement of the Corrosion Rate of Magnesium Alloys: Brief Review and Challenges. *Metals* **2020**, *10*, 775. https://doi.org/10.3390/met10060775
14. Khalili, M.A., Tamjid, E. Controlled biodegradation of magnesium alloy in physiological environment by metal organic framework nanocomposite coatings. *Sci Rep* **2021**, *11*, 8645. doi.org/10.1038/s41598-021-87783-x
15. Simchen, F.; Sieber, M.; Kopp, A.; Lampke, T. Introduction to Plasma Electrolytic Oxidation—An Overview of the Process and Applications. *Coatings* **2020**, *10*, 628. doi.org/10.3390/coatings10070628
16. Sikdar, S.; Menezes, P.V.; Maccione, R.; Jacob, T.; Menezes, P.L. Plasma Electrolytic Oxidation (PEO) Process—Processing, Properties, and Applications. *Nanomaterials* **2021**, *11*, 1375. doi.org/10.3390/nano11061375
17. Gnedenkov, A.S.; Sinebryukhov, S.L.; Filonina, V.S.; Gnedenkov, S.V. Hydroxyapatite-containing PEO-coating design for biodegradable Mg-0.8Ca alloy: Formation and corrosion behavior. *Journal of Magnesium and Alloys* **2022**, In press. doi.org/10.1016/j.jma.2022.12.002
18. Bordbar-Khiabani, A.; Yarmand, B.; Sharifi-Asl, S.; Mozafari, M. Improved corrosion performance of biodegradable magnesium in simulated inflammatory condition via drug-loaded plasma electrolytic oxidation coatings. *Materials Chemistry and Physics* **2020**, *239*, 122003. doi.org/10.1016/j.matchemphys.2019.122003
19. Bordbar-Khiabani, A.; Yarmand, B.; Mozafari, M. Enhanced corrosion resistance and in-vitro biodegradation of plasma electrolytic oxidation coatings prepared on AZ91 Mg alloy using ZnO nanoparticles-incorporated electrolyte. *Surface and Coatings Technology* **2019**, *360*, 153-171. doi.org/10.1016/j.surfcoat.2019.01.002
20. Alateyah, A.I.; Aljohani, T.A.; Alawad, M.O.; Elkatatny, S.; El-Garaihy, W.H. Improving the Corrosion Behavior of Biodegradable AM60 Alloy through Plasma Electrolytic Oxidation. *Metals* **2021**, *11*, 953. doi.org/10.3390/met11060953
21. Wu, Z.; Luo, J.; Zhang, J.; Huang, H.; Xie, Z.; Xie, X. Silver-Releasing Micro-/Nanoporous Coating on Additively Manufactured Macroporous Ti-Ta-Nb-Zr Scaffolds with High Osseointegration and Antibacterial Properties. *Coatings* **2021**, *11*, 716. doi.org/10.3390/coatings11060716
22. He, J.; Zhang, B.; Shao, L.; Feng, W.; Jiang, L.; Zhao, B. Biomechanical and histological studies of the effects of active zinc-coated implants by plasma electrolytic oxidation method on osseointegration in rabbit osteoporotic jaw. *Surface and Coatings Technology* 2020, *396*, 125848. doi.org/10.1016/j.surfcoat.2020.125848
23. He, X.; Zhang, G.; Zhang, H.; Hang, R.; Huang, X.; Yao, X.; Zhang, X. Cu and Si co-doped microporous TiO2 coating for osseointegration by the coordinated stimulus action. *Applied Surface Science* **2020**, *503*, 144072. doi.org/10.1016/j.apsusc.2019.144072
24. Lu, X.; Wu, Z.; Xu, K.; Wang, X;. Wang, S.; Qiu, H.; Li, X.; Chen, J. Multifunctional Coatings of Titanium Implants Toward Promoting Osseointegration and Preventing Infection: Recent Developments. *Front. Bioeng. Biotechnol*. **2021**, *9*, 783816. doi.org/10.3389/fbioe.2021.783816
25. Tanase, C.E.; Golozar, M.; Best, S.M.; Brooks, R.A. Cell response to plasma electrolytic oxidation surface-modified low-modulus β-type titanium alloys. *Colloids and Surfaces B: Biointerfaces* **2019**, *176*, 176-184. doi.org/10.1016/j.colsurfb.2018.12.064
26. Kaseem, M.; Hussain, T.; Ur Rehman, Z.; Ko, Y.G. Stabilization of AZ31 Mg alloy in sea water via dual incorporation of MgO and WO3 during micro-arc oxidation. *Journal of Alloys and Compounds* **2021**, *853*, 157036. doi.org/10.1016/j.jallcom.2020.157036
27. Hao, G.; Zhang, D.; Lou, L.; Yin, L. High-temperature oxidation resistance of ceramic coatings on titanium alloy by micro-arc oxidation in aluminate solution. *Progress in Natural Science: Materials International* **2022**, *32*, 401-406. doi.org/10.1016/j.pnsc.2022.06.001
28. Sedelnikova, M.B.; Ivanov, K.V.; Ugodchikova, A.V.; Kashin, A.D.; Uvarkin, P.V.; Sharkeev, YuP.; Tolkacheva, T.V.; Tolmachev, A.I.; Schmidt, J.; Egorkin, V.S.; Gnedenkov, A.S. The effect of pulsed electron irradiation on the structure, phase composition, adhesion and corrosion properties of calcium phosphate coating on Mg0.8Ca alloy. *Materials Chemistry and Physics* **2023**, *294*, 126996. doi.org/10.1016/j.matchemphys.2022.126996

29. Rokosz, K.; Hryniewicz, T.; Dudek, Ł. Phosphate Porous Coatings Enriched with Selected Elements via PEO Treatment on Titanium and Its Alloys: A Review. *Materials* **2020**, *13*, 2468. doi.org/10.3390/ma13112468
30. Wu, T.; Blawert, C.; Serdechnova, M.; Karlova, P.; Dovzhenko, G.; Wieland, D.C.F.; Stojadinovic, S.; Vasilic, R.; Wang, L.; Wang, C.; Mojsilovic, K.; Zheludkevich, M.L. Role of phosphate, silicate and aluminate in the electrolytes on PEO coating formation and properties of coated Ti6Al4V alloy. *Applied Surface Science* **2022**, *595*, 153523. doi.org/10.1016/j.apsusc.2022.153523
31. Toulabifard, A.; Rahmati, M.; Raeissi, K.; Hakimizad, A.; Santamaria, M. The Effect of Electrolytic Solution Composition on the Structure, Corrosion, and Wear Resistance of PEO Coatings on AZ31 Magnesium Alloy. *Coatings* **2020**, *10*, 937. doi.org/10.3390/coatings10100937
32. Sedelnikova, M.B.; Sharkeev, Yu.P.; Tolkacheva, T.V.; Uvarkin, P.V.; Chebodaeva, V.V.; Prosolov, K.A.; Bakina, O.V.; Kashin, A.D.; Shcheglova, N.A.; Panchenko, A.A.; Krasovsky, I.B.; Solomatina, M.V.; Efimenko, M.V.; Pavlov, V.V.; Cherdantseva, L.A.; Kirilova, I.A. Additively manufactured porous titanium 3D–scaffolds with antibacterial Zn-, Ag- calcium phosphate biocoatings. *Materials Characterization* **2022**, *186*, 111782. doi.org/10.1016/j.matchar.2022.111782
33. Wang, J.; Pan, Y.; Feng, R.; Cui, H.; Gong, B.; Zhang, L.; Gao, Z.; Cui, X.; Zhang, H.; Jia, Z. Effect of electrolyte composition on the microstructure and bio-corrosion behavior of micro-arc oxidized coatings on biomedical Ti6Al4V alloy. *Journal of Materials Research and Technology* **2020**, *9*, 1477-1490. doi.org/10.1016/j.jmrt.2019.11.073
34. Yao, W.; Wu, L.; Wang, J.; Jiang, B.; Zhang, D.; Serdechnova, M.; Shulha, T.; Blawert, C.; Zheludkevich, M.L.; Pan, F. Micro-arc oxidation of magnesium alloys: A review. *Journal of Materials Science & Technology* **2022**, *118*, 158-180. doi.org/10.1016/j.jmst.2021.11.053
35. Sedelnikova, M.; Bakina, O.; Ugodchikova, A.; Tolkacheva, T.; Khimich, M.; Uvarkin, P.; Kashin, A.; Miller, A.; Egorkin, V.; Schmidt, J.; Sharkeev, Y. The Role of Microparticles of β-TCP and Wollastonite in the Creation of Biocoatings on Mg0.8Ca Alloy. *Metals* **2022**, *12*, 1647. doi.org/10.3390/met12101647
36. Wang, F.; Wang, X.; Xie, E.; Wang, F.; Gan, Q.; Ping, S.; Wei, J.; Li, F.; Wang, Z. Simultaneous incorporation of gallium oxide and tantalum microparticles into micro-arc oxidation coating of titanium possessing antibacterial effect and stimulating cellular response. *Biomaterials Advances* **2022**, *135*, 212736. doi.org/10.1016/j.bioadv.2022.212736
37. Li, Z.; Cai, Z.; Ding, Y.; Cui, X.-J.; Yang, Z.; Zhu, M. Characterization of graphene oxide/ZrO2 composite coatings deposited on zirconium alloy by micro-arc oxidation. *Applied Surface Science* **2020**, *506*, 144928. doi.org/10.1016/j.apsusc.2019.144928
38. R. Askarnia, M. Sobhani, M. Zare, H. Aghamohammadi, H. Staji, Incorporation of Al2O3 and ZrO2 ceramics to AZ31 magnesium alloys composite coating using micro-arc oxidation method. *Journal of the Mechanical Behavior of Biomedical Materials* **2023**, *141*, 105784. doi.org/10.1016/j.jmbbm.2023.105784
39. Yang, W.; Wu, S.; Xu, D.; Gao, W.; Yao, Y.; Guo, Q.; Chen, J. Preparation and performance of alumina ceramic coating doped with aluminum nitride by micro arc oxidation. *Ceramics International* **2020**, *46*, 17112-17116. doi.org/10.1016/j.ceramint.2020.03.179
40. Molaeipour, P.; Allahkaram, S.R.; Akbarzadeh, S. Corrosion inhibition of Ti6Al4V alloy by a protective plasma electrolytic oxidation coating modified with boron carbide nanoparticles. *Surface and Coatings Technology* **2022**, *430*, 127987. doi.org/10.1016/j.surfcoat.2021.127987
41. Chebodaeva, V.V.; Sedelnikova, M.B.; Kashin, A.D.; Bakina, O.V.; Khlusov, I.A.; Zharin, A.L.; Egorkin, V.S.; Vyaliy, I.E.; Sharkeev, Yu.P. Structure and electrical potential of calcium phosphate coatings modified with aluminum oxyhydroxide nanoparticles. *Letters on Materials* **2022**, *12*, 336-342. doi.org/10.22226/2410-3535-2022-4-336-342
42. Wang, X.; Ju, P.; Lu, X.; Chen, Y.; Wang, F. Influence of Cr2O3 particles on corrosion, mechanical and thermal control properties of green PEO coatings on Mg alloy. *Ceramics International* **2022**, *48*, 3615-3627. doi.org/10.1016/j.ceramint.2021.10.142
43. Vaghefinazari, B.; Lamaka, S.V.; Blawert, C.; Serdechnova, M.; Scharnagl, N.; Karlova, P.; Wieland, D.C.F.; Zheludkevich, M.L. Exploring the corrosion inhibition mechanism of 8-hydroxyquinoline for a PEO-coated magnesium alloy. *Corrosion Science* **2022**, *203*, 110344. doi.org/10.1016/j.corsci.2022.110344
44. Kashin, A.D.; Sedelnikova, M.B.; Chebodaeva, V.V.; Uvarkin, P.V.; Luginin, N.A.; Dvilis, E.S.; Kazmina, O.V.; Sharkeev, Yu.P.; Khlusov, I.A.; Miller, A.A.; Bakina, O.V. Diatomite-based ceramic biocoating for magnesium implants. *Ceramics International* **2022**, *48*, 28059-28071. doi.org/10.1016/j.ceramint.2022.06.111
45. Fattah-alhosseini, A.; Chaharmahali, R.; Babaei, K. Effect of particles addition to solution of plasma electrolytic oxidation (PEO) on the properties of PEO coatings formed on magnesium and its alloys: A review. *Journal of Magnesium and Alloys* **2020**, *8*, 799-818. doi.org/10.1016/j.jma.2020.05.001
46. D.V. Mashtalyar, I.M. Imshinetskiy, K.V. Nadaraia, A.S. Gnedenkov, S.N. Suchkov, D.P. Opra, E.V. Pustovalov, A. Yu Ustinov, S.L. Sinebryukhov, S.V. Gnedenkov, Effect of TiO2 nanoparticles on the photocatalytic properties of PEO coatings on Mg alloy. *Journal of Magnesium and Alloys* **2023**, *11*, 735-752. doi.org/10.1016/j.jma.2022.10.021
47. Mozafarnia, H.; Fattah-Alhosseini, A.; Chaharmahali, R.; Nouri, M.; Keshavarz, M.K.; Kaseem, M. Corrosion, Wear, and Antibacterial Behaviors of Hydroxyapatite/MgO Composite PEO Coatings on AZ31

 doi:10.20944/preprints202306.0150.v1

Mg Alloy by Incorporation of TiO2 Nanoparticles. *Coatings* **2022**, *12*, 1967. doi.org/10.3390/coatings12121967

48. Molaei, M.; Fattah-alhosseini, A.; Nouri, M.; Mahmoodi, P.; Nourian, A. Incorporating TiO2 nanoparticles to enhance corrosion resistance, cytocompatibility, and antibacterial properties of PEO ceramic coatings on titanium. *Ceramics International* **2022**, *48*, 21005-21024. doi.org/10.1016/j.ceramint.2022.04.096
49. Ignjatović, S.; Blawert, C.; Serdechnova, M.; Karpushenkov, S.; Damjanović, M.; Karlova, P.; Wieland, D.C.F.; Starykevich, M.; Stojanović, S.; Damjanović-Vasilić, L.; Zheludkevich, M.L. Formation of multi-functional TiO2 surfaces on AA2024 alloy using plasma electrolytic oxidation. *Applied Surface Science* **2021**, *544*, 148875. doi.org/10.1016/j.apsusc.2020.148875
50. Hashemzadeh, M.; Raeissi, K.; Ashrafizadeh, F.; Hakimizad, A.; Santamaria, M. Incorporation mechanism of colloidal TiO2 nanoparticles and their effect on properties of coatings grown on 7075 Al alloy from silicate-based solution using plasma electrolytic oxidation. *Transactions of Nonferrous Metals Society of China* **2021**, *31*, 3659-3676. doi.org/10.1016/S1003-6326(21)65755-2
51. Sedelnikova, M.B.; Kashin, A.D.; Uvarkin, P.V.; Tolmachev, A.I.; Sharkeev, Y.P.; Ugodchikova, A.V.; Luginin, N.A.; Bakina, O.V. Porous Biocoatings Based on Diatomite with Incorporated ZrO_2 Particles for Biodegradable Magnesium Implants. *J. Funct. Biomater.* **2023**, *14*, 241. doi.org/10.3390/jfb14050241